




# Sodium–tungsten–titanium phosphate glasses: an investigation of the structure, chemical endurance, and kinetic characteristics

Hicham Es-soufi<sup>1,\*</sup> , M. I. Sayyed<sup>2,3</sup>, and Lahcen Bih<sup>1</sup>

<sup>1</sup>Laboratory of Engineering Sciences and Professions, Materials and Processes Department ENSAM-Meknes Marjane II, Moulay Ismail University, El Mansour, P.O. Box 15290, Meknes, Morocco

<sup>2</sup>Department of Physics, Faculty of Science, Isra University, Amman 11622, Jordan

<sup>3</sup>Department of Nuclear Medicine Research, Institute for Research and Medical Consultations, Imam Abdulrahman Bin Faisal University, Dammam 31441, Saudi Arabia

Received: 19 April 2023

Accepted: 29 May 2023

Published online:

16 June 2023

© The Author(s), under exclusive licence to Springer Science+Business Media, LLC, part of Springer Nature 2023

## ABSTRACT

Many technologies have applied sodium ions' solid electrolytes, ranging from batteries to chemical sensors. This study investigated phosphate glasses featuring electrolyte developed through the  $20\text{Na}_2\text{O}-(50-x)\text{Na}_2\text{WO}_4-x\text{TiO}_2-30\text{P}_2\text{O}_5$  system (with  $0 \leq x \leq 25$  mol%), with the melt-quenching approach employed. For the estimation of the activation energy, differential scanning calorimetry was utilized, whereby crystallization ( $E_c$ ) was relied upon.  $E_c = 144.77$  kJ/mol characterized the glass ( $x = 5$ ). The determination of the crystallization mechanism was possible through the Avrami parameter ( $n$ ), which was found to be approximately  $\approx 2$ ; therefore, the crystallization mechanism was expected to be a periodic landscape that is one-dimensional in nature. The bonds forming the glasses' framework were shown to be established through the  $\text{PO}_4$  units, as revealed by Raman spectroscopy.  $\text{TiO}_2$  insertion into the framework of glass resulted in new bond formation, namely P–O–Ti and/or Ti–O–Ti. Shifting the  $\text{Na}_2\text{WO}_4$  mol% to  $\text{TiO}_2$  mol% resulted in the structural units' transformation into  $\text{Q}^2$ ,  $\text{Q}^1$ , and finally  $\text{Q}^0$  units. Through the durability analysis, the results confirmed that the explored glasses' dissolution is reliant upon their composition, which is of a glassy nature. There is an increase in durability when  $\text{Na}_2\text{WO}_4$  is replaced by  $\text{TiO}_2$ .

Address correspondence to E-mail: hichamessoufi@gmail.com

## 1 Introduction

Phosphate glasses have been the focus of research in recent decades. Because phosphate glasses have several advantages over other glasses, these advantages are manifested in the following: the diversity of properties (electrical, optical, magnetic, etc.); good thermal stability; structural diversity; storage of a large number of oxides; speed of preparation; etc. For example, phosphate glasses of sodium are promising solid electrolytes for electro-optic applications [1–4]. Glasses composed of sodium phosphate are broadly accepted to be characterized, in general, in terms of their weak chemical stability. Therefore, the parameter of chemical durability in solid electrolytes is perceived as a vital determinant. Research has found that the glass–water reaction results in two phases: (1) the exchange of an ionic nature among the  $\text{Na}^+$  proximate to non-bridging oxygens (NBOs) with the protonated species during the diffusion process, which is proportional to  $t^{1/2}$  and (2) the P–O–P chain phosphates' rupture during the hydrolysis process, which is dependent on time ( $t$ ) [5–7]. The solubleness of the metal oxide-containing phosphate glasses facilitates the investigation of their impact on their chemical, mechanical, and physical properties [8–13]. Additionally, the ability of metals' incorporation to enhance phosphate glasses' durability has been widely reported [14, 15]. In particular, such glasses reflect a universal issue that is grounded in its limited solubleness. The influence of metal oxides on phosphate glasses' physico-chemical and structural properties has been investigated in this context, whereby the metals' insertion was found to improve the studied glasses' durability. Considerable consideration has more recently been given to titanium due to the phosphate framework that functions as an effective stabilizer through the replacement of P–O–P bonds with Ti–O–P bonds [16–18]. Glassy phosphates' degradability being effectively enhanced by titanium dioxide has been widely reported [19–22]. Titanium oxide, as is well known, has an intermediary function (former or modifier), although it is unable to form glass independently [17]. The host glass's characteristics and structure can be easily modified by the titanium ion due to its differentiation by ionic size, which is characterized as small [23]. Moreover, the existence of titanium comprises dual valence states: tetravalent  $\text{Ti}^{4+}$  that is absent of color and the purple trivalent  $\text{Ti}^{3+}$  [23]. Titanium Ti tends

to exist in structural phosphate as a six-, five-, and four-coordinated form [17]. Numerous publications extensively discuss the glassy phosphates of titanium and their potential applications. These glasses are notable for their properties, including electrical, magnetic, and optical characteristics, which can be attributed to the presence of titanium phosphate [23].

Furthermore, tungsten phosphate glasses represent useful materials as they exhibit satisfactory electrochromic, gasochromic, and photochromic properties [24]. Typically, glasses in binary systems can be formed with elevated  $\text{WO}_3$  in the 60 to 75 mol% range, for instance,  $\text{GeO}_2$ ,  $\text{B}_2\text{O}_3$ , and  $\text{P}_2\text{O}_5$ . A stable binary  $\text{P}_2\text{O}_5$ – $\text{WO}_3$  is formed when the  $\text{WO}_3$  content is allowed to reach  $\leq 80$  mol% [24]. The analysis of glasses featuring  $\text{WO}_3$  revealed that tungsten ions exist in the octahedral coordination [25]. Moreover, the  $\text{PO}_4$  tetrahedra and  $\text{WO}_6$  octahedra were shown through structural research to share their corners in the binary system of glasses composed of tungsten phosphate. Nevertheless, the glasses characterized by  $\text{WO}_3$  of 80 mol% are unstable since they are dominated by corner-shared octahedrals, with such glasses having a susceptibility for crystallizing [25], although the  $\text{SbPO}_4$ – $\text{WO}_3$  glassy system offers satisfactory stability as well as an optimum index for refraction [26]. Through the structural data, two glass frameworks can be determined based on the  $\text{WO}_6$  octahedra: (1) those with emphasis on traversing the  $\text{PO}_4$  tetrahedral with the  $\text{WO}_6$  octahedral at the structure's forward end and (2) those that jointly form, when there is an increase in  $\text{WO}_3$  through the two  $\text{WO}_6$  octahedrals [26]. Vitrification of the glassy phosphates is conducted over a wide composition range in the  $\text{P}_2\text{O}_5$ – $\text{WO}_3$ – $\text{A}_2\text{O}$  ternary diagrams ( $A = \text{Na}, \text{Li}$ ). The  $\text{P}_2\text{O}_5$ – $\text{A}_2\text{MO}_4$ – $\text{A}_2\text{O}$  ternary system's ( $M = \text{Mo}, \text{W}; A = \text{Li}, \text{Na}$ ) altered glassy phosphates were structurally explored via electron paramagnetic resonance (EPR), infrared, and Raman spectroscopies. Depending on the glassy composition, these glasses have  $\text{MO}_6$  octahedral,  $\text{MO}_4$  tetrahedral,  $\text{M}_2\text{O}_7$  dimers,  $\text{PO}_4$  and  $\text{P}_2\text{O}_7$  units, or metaphosphate chains, in their structure. The depolymerization of the vitreous framework occurs when there is an increase in  $\text{A}_2\text{O}$ . EPR investigations were carried out on X-ray diffraction irradiated and non-irradiated samples [27, 28] and  $y\text{A}_2\text{O}-(1-y)[0.25(\text{WO}_3)_2-0.75\text{P}_2\text{O}_5]$  series glasses are produced,  $y = 0.10$ – $0.60$  mol%. It is revealed by differential thermal analysis experiments that

increased modifier content breaks the glassy network. The EPR spectra reveal two signals that are dependent on the  $W^{5+}$  and  $Mo^{5+}$  ions. With increased  $A_2O$ , the EPR centers' intensity reduces. There is an association between decreasing  $T_g$  with the oxide modifier amount and the changes of a structural nature that result in the glasses compositions' matrix [27].

This study aims to look into the effects of  $TiO_2$  on phosphate glasses' chemical resistance  $20Na_2O-(50-x)Na_2WO_4-xTiO_2-30P_2O_5$  ( $x = 0-25$  mol%). In addition, bringing fresh perspectives to bear on the mechanisms of dissolution, particularly as they relate to the transition between the two stages ( $t < t_{trans}$  and  $t > t_{trans}$ ) of dissolution, in order to explain the conclusions that were reached.

## 2 Materials and procedures

### 2.1 Glass preparation

The conventional melt-quenching route was utilized to prepare phosphate glasses through  $20Na_2O-(50-x)Na_2WO_4-xTiO_2-30P_2O_5$  ( $x = 0, 1, 5, 8, 10, 15, 20,$  and  $25$  mol%). Based on their molar compositions, the first stage was to weigh and thoroughly mix the  $Na_2CO_3$ ,  $Na_2WO_4$ ,  $TiO_2$ , and  $NH_4H_2PO_4$  precursors (purchased from Sigma-Aldrich in the USA). The next step was to deposit the mixture in an alumina crucible, which was then inserted into an electric furnace heated first at  $300$  °C for 12 h, followed by  $500$  °C for 1 h. In order to achieve the melt, the furnace's temperature was then raised, with stirring carried out for approximately one hour at  $900$  °C to attain homogenization. After that, the melt was air-quenched to realize the glasses that were annealed for one hour at  $300$  °C and then cooled within the furnace until they reached room temperature. Since the resulting glasses were colorless and transparent due to the process, prior to use, they were placed into desiccators. An X-ray diffractometer was employed to analyze the resulting glasses' amorphous state, with confirmation attained through Raman spectroscopy.

### 2.2 Glasses' characterization

In order to review the prepared glasses' phosphate units' structural framework, the Raman approach was employed. A LabRam HR spectrometer (Horiba

Jobin Yvon) was used to collect Raman data at room temperature. In backscattering geometry, analysis of the spectra was carried out under the excitation condition utilizing He-Ne laser radiation ( $632.8$  nm,  $12$  mW): accumulated number ( $10$ ), exposure time ( $3$  s), and width of spectral slit ( $1$  mm).

The determination of the developed glasses' chemical durability data was attained through dissolution tests in  $30$  °C demineralized water. The resultant glasses were shaped into blocks and placed in a bottle containing demineralized water with a pH of  $6.70$ . The bottles were placed in a thermostatic bath at  $30$  °C for 240 h. Equation (1) is used to compute the percentage of dissolution ( $D_R$ ) (s.t) [29]:

$$D_R = \frac{D_x}{S}, \quad (1)$$

where  $D_x$  refers to the loss of mass (g),  $S$  indicates the surface of the sample ( $cm^2$ ), and  $t$  denotes the immersion time (h). A pH meter was used to establish each glass's leaching solution's pH after determining the dissolution rate every 24 h.

The collection of the crystallization kinetics data was achieved using differential scanning calorimetry in the  $30-575$  °C temperature range. First, grinding was carried out so that the synthesized glasses became a fine ( $50$  μm) powder. After that,  $40$  mg of the powder was inserted into an alumina crucible, with temperatures of  $5, 8, 10,$  and  $12$  °C/min applied. The maximum crystallization temperature ( $T_p$ ) value at the respective rates  $\beta$  (°C/mn<sup>-1</sup>) was fixed using the gathered data.

## 3 Results and discussion

### 3.1 Raman spectroscopy

Figure 1 shows the results of the Raman scattering spectroscopy in the range of  $1200-150$   $cm^{-1}$ , which was used to investigate the prepared glassy phosphates' structure of the  $20Na_2O-(50-x)Na_2WO_4-xTiO_2-30P_2O_5$  system ( $x = 0, 1, 5, 8, 10, 15, 20,$  and  $25$  mol%). According to the literature [30–32], the Raman spectra bands are assigned. Consequently, Table 1 presents the primary positions and assignments of the bands at  $1095, 935, 885, 750, 650-570, 390,$  and  $255$   $cm^{-1}$ . Figure 1 reveals the location of the primary bands in the  $935-750$   $cm^{-1}$  range, which on differing P-tetrahedra are related to NBO's

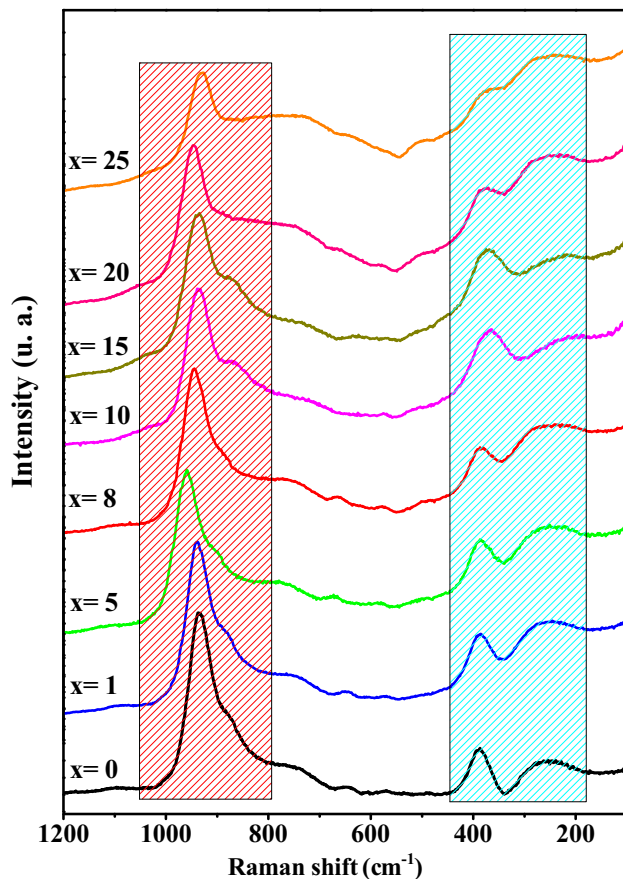


**Fig. 1** Raman spectra of the studied glasses

**Table 1** Raman band assignments in the 1200–150  $\text{cm}^{-1}$  range frequency for the studied phosphate glasses

Band position ( $\text{cm}^{-1}$ )	Band assignment
1095	$\nu_s(\text{PO}_2)^-, \text{Q}^2$
935	$\nu_{\text{as}}(\text{P-O-P})/\nu_{\text{as}}(\text{P-O-M})$ ( $M = \text{W, Ti}$ )
885	$\text{O-M-O}/\text{MO}_4/\text{MO}_6$ ( $M = \text{W, Ti}$ )
750	$\nu_s(\text{P-O-P}), \text{Q}^1$
650–570	$\nu_s(\text{P-O-P}), \text{Q}^2$
390	$\nu_s(\text{M-O-M})$ ( $M = \text{W, Ti}$ )
255	$\delta(\text{PO}_4)$

symmetric and asymmetric vibration modes. Moreover, on three-dimensional phosphates ( $\text{Q}^2$ ),  $\text{P}_2\text{O}_7$  ( $\text{Q}^1$ ) dimers, and isolated  $\text{PO}_4$  ( $\text{Q}^0$ ), the P–O bonds' peak frequency experiences a systematic decrease. The band in the  $885 \text{ cm}^{-1}$  region is linked with the  $\text{WO}_6$ 's W–O and/or W–O–P bond's symmetric mode of vibration. At  $750 \text{ cm}^{-1}$ , the low intensity band is linked with the symmetric mode of vibration of the  $\text{Q}^1$  units' P–O–P bond that is additionally presented.

The low-region bands positioned in the  $650\text{--}255 \text{ cm}^{-1}$  range are typically attributed to the  $\text{PO}_4$  units' stretching modes. Within the system, even after the substitution of  $\text{Na}_2\text{WO}_4$  by  $\text{TiO}_2$ , a significant change in the spectra became apparent in terms of the  $\text{TiO}_2$  content increase. The  $935$  and  $885 \text{ cm}^{-1}$  supplementary bands' dependence on  $\text{TiO}_4$  and  $\text{TiO}_6$ , respectively, could be noted from the composition ( $x = 1 \text{ mol\%}$ ). With increased  $\text{TiO}_2$  mol%, there was a decrease in intensity (see the red zone in Fig. 1) [33]. With an increase in  $\text{TiO}_2$  content, there was a decrease in the relative intensity of the  $\text{Q}^1$ -attributed peak. Moreover, the  $450\text{--}180 \text{ cm}^{-1}$  band intensity appeared to begin to decrease with increased  $\text{TiO}_2$  quantity (see the green zone in Fig. 1). With an increase in  $\text{TiO}_2$  content to 5 mol% and above, the intensity of the  $1095 \text{ cm}^{-1}$  band was noted to decrease with the  $\text{TiO}_2$  quantity. There is an association between the  $1050$  and  $1095 \text{ cm}^{-1}$  range vibrations and the symmetric mode's vibration of the NBOs in the pyrophosphate structural units  $(\text{P}_2\text{O}_7)_4^-$  [34]. A  $650 \text{ cm}^{-1}$  band was noted in the lower wavenumber region, where decreased intensity accompanied increased  $\text{TiO}_2$  content. There is thus the potential for the Ti–O bonds' vibration mode to be controlled in the  $\text{TiO}_6$  octahedral units [35], the prediction of which is grounded in the presence in differing glassy frameworks of a number of structural units. It has been suggested that the distorted octahedrals could occupy the titanium ions, thus contributing to the glassy matrix's modification, which is followed by the increase in NBOs. Due to the presence of elevated quantities ( $x > 5$ ) of  $\text{TiO}_2$  mol%,  $\text{TiO}_4$ 's structural units rupture the P=O bonds, thus leading to the formation of NBO ions and structural units  $[\text{TiO}_{6/2}]^2$  [36]. Furthermore, there is an increase in  $\text{TiO}_6$  structural units with elevated quantities of  $\text{TiO}_2$ . The vibration intensity-produced Raman spectra identify a significant reduction in the metaphosphate  $\text{Q}^2$  units as far as  $x = 8 \text{ mol\%}$ , while there is a predomination for the pyrophosphate  $\text{Q}^1$  units at  $x \geq 8$ , as shown by the analysis in Fig. 1. However, it is challenging to determine the precise  $\text{Q}^1$  and  $\text{Q}^2$  unit quantities, since it requires using  $^{31}\text{P}$  MAS-NMR. The Ti–O bonds' elevated polarizability in comparison with the P–O bonds is impacted by the Raman bands' intensity. Irrespective of the  $\text{TiO}_2$  increase to 20 and 25 mol%, glassy phosphates can still be found that feature the metaphosphate  $\text{Q}^2$  units [35]. The assumption is that within the glassy framework,

elevation of the TiO<sub>2</sub> mol% resulted in a partial shift of the metaphosphate into a pyrophosphate, followed by an orthophosphate structure. At TiO<sub>2</sub> ( $x < 8$  mol%), there is a predominance of the metaphosphate units within the glassy structure. Subsequently, the pyrophosphate as well as the orthophosphate units will be elevated. Consequently, there is an interlinking of TiO<sub>6</sub> units with metaphosphate, orthophosphate, and pyrophosphate units, whereby P–O–Ti bonds form that become involved in increasing the prepared glasses' durability (see Sect. 3.2).

### 3.2 Chemical resistance

#### 3.2.1 Dissolution

Figure 2a presents the data gathered through the dissolution tests, where the time (h) governs the

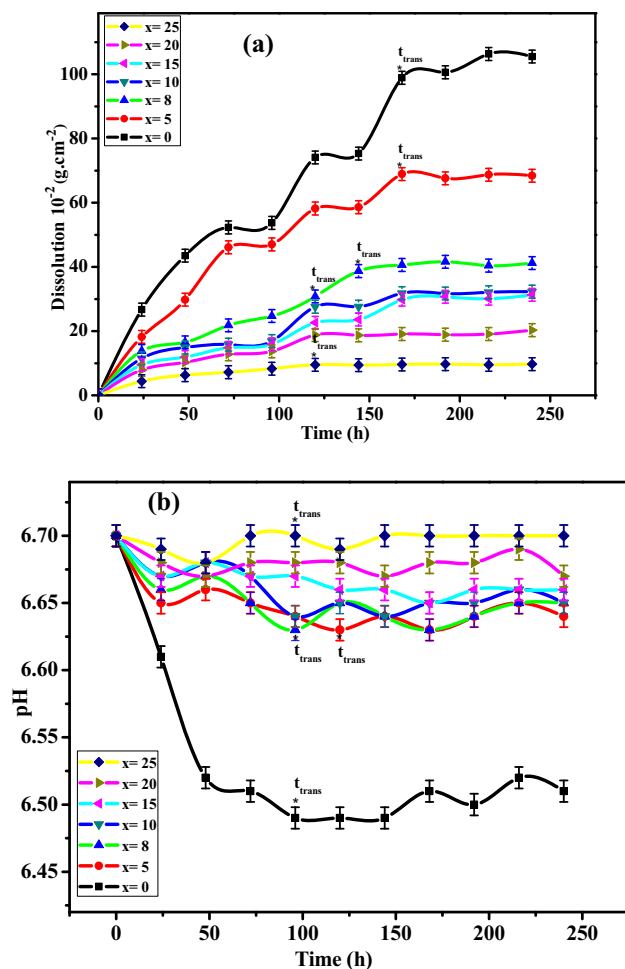


**Fig. 2** Evolution of the dissolution (a) and pH (b) of the glasses as a function of time (h)

dissolution (g) at the initial surface (cm<sup>2</sup>), where it was observed that all samples have the same dissolution behavior (see Fig. 2a). From the dissolution behavior of these samples, it could be possible to separate two stages of dissolution in similarity to Ma et al.'s work [37]. The first stage was before transition time ( $t < t_{trans}$ ). This stage was controlled by interdiffusion and hydrolysis mechanisms (Fig. 3a), which resulted in the conversion layer's formation involving the reaction of solid-state crosslinked phosphate glass anions with glass-diffused reactants, like H<sub>2</sub>O and H<sup>+</sup>. At the glass surface, there is the occurrence of dissolution, with a shift of the interface in the direction of the center, which leads to a shrinkage of the unreacted layer and a decreased surface and thus the time-based reaction area was noticeable in Fig. 3a. Through this phase, the dissolution was dominant, and the dissolution decreased from  $0-100 \times 10^{-2} \pm 0.02 \text{ g cm}^{-2}$  ( $x = 0$  mol%) to  $0-9 \times 10^{-2} \pm 0.02 \text{ g cm}^{-2}$  ( $x = 25$  mol%) (see Table 2). The glass composition also affects how things dissolve. Also, in this stage, the dissolution dependence time [38, 39] could explain this by decreasing the dissolution with increasing TiO<sub>2</sub> mol% so that the formation of the conversion layer does not develop more due to the P–O–Ti bonds' formation. A slower rate of dissolution, however, marked the second stage when  $t > t_{trans}$ . The dissolution was found independent at the time. This independence on the time could be explained by the formation of the protective layer, which limits the conversion layer as shown in Fig. 3a. But the dissolution rates decreased from  $100 \times 10^{-2} \pm 0.02 \text{ g cm}^{-2}$  at  $x = 0$  mol% to  $9 \times 10^{-2} \pm 0.02 \text{ g cm}^{-2}$  at  $x = 25$  mol% with increasing of TiO<sub>2</sub> mol% (see Table 2). Because at high TiO<sub>2</sub> mol% the protective layer rapidly forms, there was a limited dissolution rate.

In terms of substituting Na<sub>2</sub>WO<sub>4</sub> with TiO<sub>2</sub>, the synthesized glass banks' dissolution behavior on the TiO<sub>2</sub> mol% was verified. At the glassy composition's ( $x = 0$  mol%) initial dissolution phase, there was a more rapid dissolution when compared to the remaining glassy compositions ( $x > 0$  mol%). Therefore, it is possible to conclude that Na<sub>2</sub>WO<sub>4</sub>'s substitution by TiO<sub>2</sub> has an impact on the studied glasses' solubleness. Moreover, inserting TiO<sub>2</sub> mol% into the glassy phosphate led to an improvement in the glassy framework's durability. Earlier work reported that certain oxides, such as Fe<sub>2</sub>O<sub>3</sub> and TiO<sub>2</sub>, improve glassy phosphates' durability [14, 15],

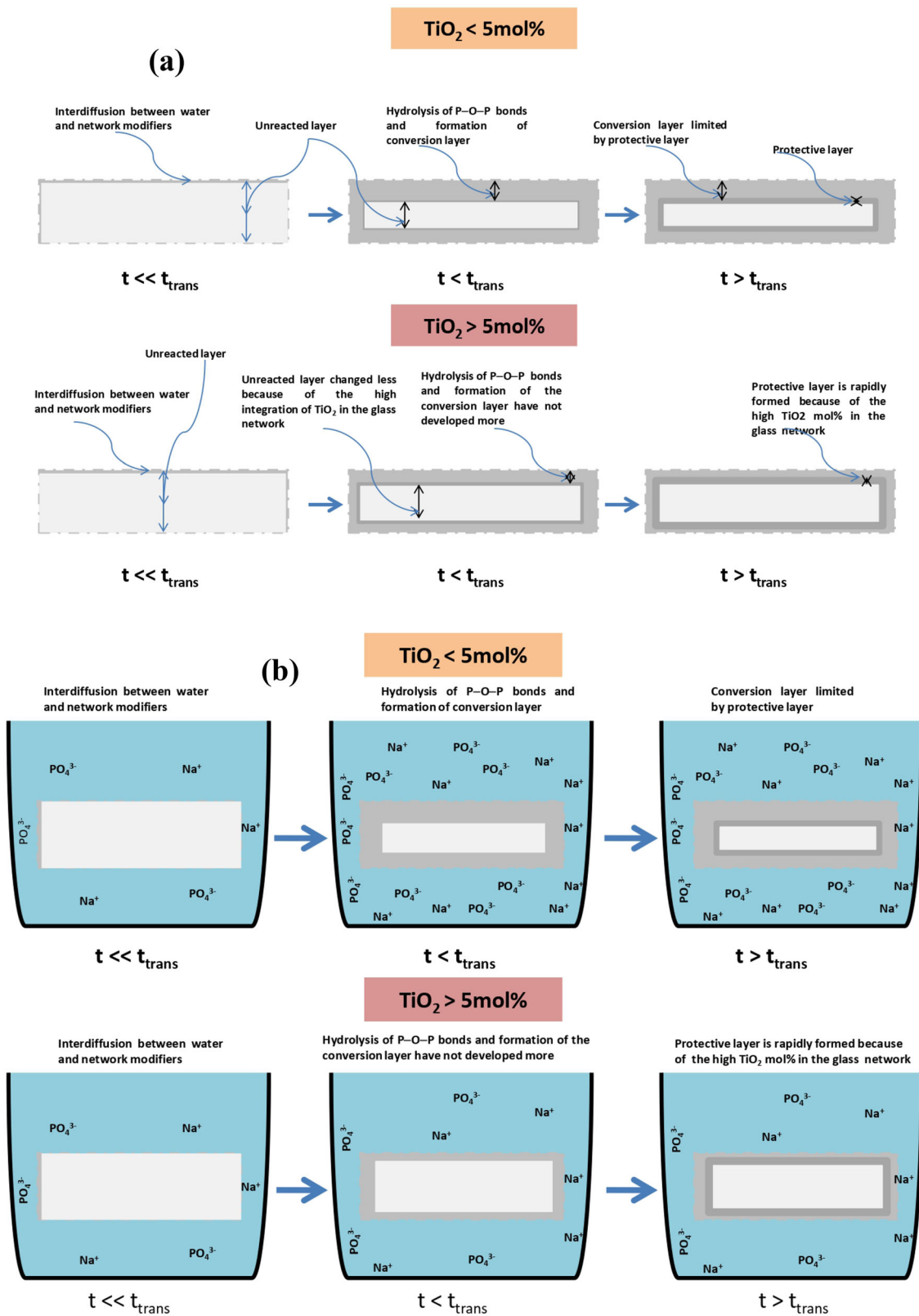


**Fig. 3** Schematic of glass dissolution and two-stage concept of glass dissolution (a), and schematic diagram the dissolution mechanism, with surface reaction-limited dissolution following  $t_{trans}$  when the protective layer forms and diffusion-limited dissolution prior to  $t_{trans}$  (b)

**Table 2** Data of the dissolution during a time (h) for the prepared glasses

Composition x	$t < t_{trans}$ (g cm <sup>-2</sup> )	$t > t_{trans}$ (g cm <sup>-2</sup> )
0	[0–100]10 <sup>-2</sup> (± 0.02)	≈ 100 × 10 <sup>-2</sup> (± 0.02)
5	[0–68]10 <sup>-2</sup> (± 0.02)	≈ 68 × 10 <sup>-2</sup> (± 0.02)
8	[0–40]10 <sup>-2</sup> (± 0.02)	≈ 40 × 10 <sup>-2</sup> (± 0.02)
10	[0–32]10 <sup>-2</sup> (± 0.02)	≈ 32 × 10 <sup>-2</sup> (± 0.02)
15	[0–28]10 <sup>-2</sup> (± 0.02)	≈ 28 × 10 <sup>-2</sup> (± 0.02)
20	[0–19]10 <sup>-2</sup> (± 0.02)	≈ 19 × 10 <sup>-2</sup> (± 0.02)
25	[0–9]10 <sup>-2</sup> (± 0.02)	≈ 9 × 10 <sup>-2</sup> (± 0.02)

whereby the conclusion was drawn that Fe<sub>2</sub>O<sub>3</sub> or TiO<sub>2</sub>'s insertion into glassy networks resulted in a durability enhancement due to the P–O–Fe/Ti bond creation, leading to a network rigidity increase. Similarly, inserting differing TiO<sub>2</sub> quantities into the glasses in the current study enhanced the glassy network's durability via P–O–Ti bond creation, as supported through Raman spectroscopy as well as the bonds' identification (P–O–Ti). Moreover, the hypothesis was affirmed through a thermal review of the difference scanning calorimetry [40], whereby there was an increase in *T<sub>g</sub>* when TiO<sub>2</sub> was integrated into glassy networks. TiO<sub>2</sub>'s insertion into glasses promotes the strengthening of the links that form in the Na<sub>2</sub>O–Na<sub>2</sub>WO<sub>4</sub>–TiO<sub>2</sub>–P<sub>2</sub>O<sub>5</sub> system's glassy network, with the chemical durability's correlation with Raman and thermal analysis supporting this explanation.

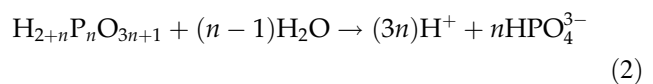
### 3.2.2 Variation in pH

Figure 2b shows the pH curves' evolution due to the period of submersion in 30 °C, demineralized water. From Fig. 2b, it could be clearly differentiated into two stages: before transition time ( $t < t_{trans}$ ) and after transition time ( $t > t_{trans}$ ). The  $t < t_{trans}$  stage is defined by a sharp pH decrease. The pH curves depend on the time, with a distinction between the studied glasses' curves from 6.70–6.50 ± 0.008 ( $x = 0$  mol%) to 6.70–6.69 ± 0.008 ( $x = 25$  mol%), as illustrated in Table 3. This suggests that the pH values' development is reliant upon the studied glassy substance's chemical composition. The pH evolution is impacted by phosphoric acid formation, which in water is survived by the H<sub>2</sub>PO<sub>4</sub><sup>-</sup> units [14]. Via the initial contact (interdiffusion mechanism), in general, the glass featuring the solution (water) and the alkali,

**Table 3** Data of the pH during a time (h) for the prepared glasses

Composition x	$t < t_{trans}$	$t > t_{trans}$
0	6.70–6.50 (± 0.008)	≈ 6.50 (± 0.008)
5	6.70–6.58 (± 0.008)	≈ 6.58 (± 0.008)
8	6.70–6.62 (± 0.008)	≈ 6.62 (± 0.008)
10	6.70–6.63 (± 0.008)	≈ 6.63 (± 0.008)
15	6.70–6.65 (± 0.008)	≈ 6.65 (± 0.008)
20	6.70–6.67 (± 0.008)	≈ 6.67 (± 0.008)
25	6.70–6.69 (± 0.008)	≈ 6.69 (± 0.008)

as well as the phosphate ions produced on the glassy surface, is percolated into the solution (see Fig. 3b). Through the hydrolysis mechanism and formation of the conversion layer, the exchange of ions between those of the solution and those that appear on the glassy surface have the potential to determine the solution's acid-based characteristic. Essentially, the pH curves' sudden decrease is linked to the phosphate units' (H<sub>2</sub>PO<sub>4</sub><sup>-</sup>) influx into the solution from the glassy surface ( $t < t_{trans}$ ). In a similar study, Oosterbeek et al. [41] suggested Eq. (2) to explain the phosphate units nPO<sub>4</sub><sup>3-</sup> and the variation of pH values through the hydrolysis of the surface of glass.



Through the second stage ( $t > t_{trans}$ ) the H<sub>2</sub>PO<sub>4</sub><sup>-</sup> units slow down because of saturation of the solution and the formation of the protective layer. For this reason, the pH curve behavior becomes independent of time (constant), as illustrated in Fig. 3b. The pH values increased from 6.50 (± 0.008) at  $x = 0$  mol% to 6.69 (± 0.008) at  $x = 25$  mol% with increasing TiO<sub>2</sub> mol% (see Table 3). In the glassy state, the glassy network was increased ( $x > 5$ ) at TiO<sub>2</sub> because of the rapid occurrence of saturation, while the TiO<sub>2</sub> quantity was raised. Consequently, the studied glasses' enhanced durability due to the TiO<sub>2</sub> mol% insertion into the glassy framework was confirmed.

In this study, two separate zones were found in the produced glasses' chemical durability: one with rapid change and the other with sluggish change. It is crucial that the pH value drops suddenly when thermodynamic disequilibrium occurs within the changing solution and glassy surface. The saturation of the shifting solution serves as a gauge for the

changing solution, where corrosion dominates. The creation of a shield against the glassy surface's diffusion led to the saturation effect. The findings of this investigation support those of Oosterbeek et al. [41]. In order to unpack the behavior of the two-stage dissolution, a new dissolution mechanism that accounts for a dissolving medium of greater complexity has been developed. In the first phase, metal hydroxides and hydrated phosphate anions form a conversion layer as ions or water permeate in a  $t^{1/2}$ -dependent manner into the glass. Layer dissolution processes become rate limiting and give rise to linear  $t$  dependence once the solution conditions slow them down to the point where the conversion layer is stabilized. According to this mechanism, the solution circumstances and the conversion layer characteristics have an impact on the transition time ( $t_{trans}$ ). In another study, it was possible to summarize water's corrosive impact on alkaline phosphate glasses composed of  $(1 - x) \text{P}_2\text{O}_5 - x \text{Na}_2\text{O}$  through two mechanisms' involvement—hydrolysis and hydration—with each having varying importance in terms of the depolymerization degree and the composition function ( $x$ ) [42]. There is an association between water diffusion and hydration, with the formation of a hydration layer. Where the glassy structure primarily comprises  $\text{Q}^2$  units that form chains, namely in the region of  $x = 0.5$  (polyphosphate and metaphosphate), hydration predominates. In general, it commences with the end of the chain that results from hydroxylated  $\text{Q}^1$  entities, providing unfettered access to the inter-chain water penetration. Hydrated chains are widely accepted to decouple from the glassy surface to allow their intact migration into the solution. Nevertheless, the mechanism of hydrolysis is defined by (1) a reaction that features low energy when the phase is inter-diffusional and has  $\text{H}^+ \leftrightarrow \text{Na}^+$  ion-exchange reaction, referred to as an "ion-exchange" or "dealkalinization," between the solution's ions and those of the  $\text{Na}^+$  found among the entities of phosphate and (2) a considerably greater energetic reaction leading to the P–O–P bond's rupture with the  $\text{H}^+$  and  $\text{OH}^-$  ions' binding, from the water dissociation. It also has particular responsibility for the ultra-phosphates' dissolution. However, there was the relief of the chains into the solution, commencing with the ends [42, 43].

### 3.3 Kinetics of crystallization

Differential scanning calorimetry thermal examination of glasses allows for their behavior to be identified as a temperature function. Information can be gathered regarding crystallization mechanisms by analyzing glasses at various speeds of heating ( $\beta$ ). We may trace the evolution of the temperature of the crystallization as a heating rate function ( $T_c = (\beta)$ ) using these non-isothermal observations. This fluctuation allowed us to determine the characteristics that characterize the materials' crystallization, such as the activation energy of the crystallization ( $E_c$ ) that is found using the Kissinger equation's specific form (1) [44] and which in terms of the analyzed glasses will be explored in order to determine the crystallization kinetics mechanism.

$$\ln\left(\frac{T_p^2}{\beta}\right) = \frac{E_c}{RT_p} + C, \quad (3)$$

where  $\beta$  refers to the heating rate  $\beta$  (5, 8, 10, and 12 °C/min),  $R$  indicates the universal gas constant,  $T_p$  is the peak temperature, and  $C$  denotes the constant.

From the activation energy ( $E_c$ ) value, it was possible to calculate the Avrami exponent ( $n$ ) through the Augis–Bennett Eq. (4) [45]:

$$n = \left(\frac{2.5}{\Delta T}\right) \times \left(\frac{RT_p^2}{E_c}\right), \quad (4)$$

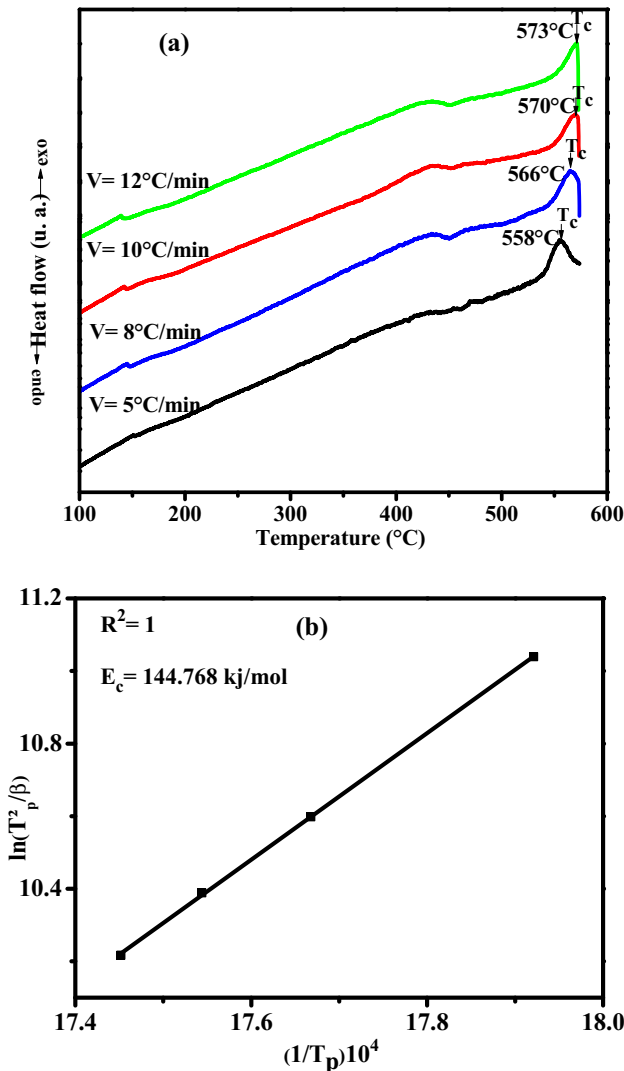
where  $n$  indicates the Avrami exponent or crystallization index and  $\Delta T$  is the entire width of the exothermic differential scanning calorimetry peak at an intensity of half the maximum. The increasing and nucleation mechanisms were indicated by the Avrami exponent ( $n$ ). In the published research, ( $n$ ) is assigned to the pattern of crystallization,  $n = 1$  indicates the crystallization surface,  $n = 2$  refers to crystallization of a mono-dimensional nature,  $n = 3$  denotes crystallization of a bi-dimensional nature, and  $n = 4$  is the crystallization in three-dimensional glassy materials [46, 47].

Figure 4a presents the differential scanning calorimetry thermograms that correspond to the glassy formulation ( $x = 5$ ) for all the proposed rates of heating. Each thermogram presenting a peak of crystallization was verified. Nevertheless, when



comparing the peaks of crystallization, a gradual shift to the higher temperature value was noted as there was an increase in heating rates. Table 4 presents the values that were obtained in terms of the synthesized glass ( $x = 5 \text{ mol\%}$ ) corresponding to temperature of crystallization ( $T_p$ ). Through examining the heating rates and crystallization temperature ( $T_p$ ), Fig. 4b

highlights the  $\ln(T_p^2/\beta)$  versus  $1/T_p$  plot. Moreover, it was possible to establish the  $E_c$  value to be approximately  $144.77 \text{ kJ/mol}$  from the variation slope, with the  $\ln(T_p^2/\beta)$  parameter as a  $1/T_p$  function. Meanwhile, the Avrami parameter ( $n$ ) was determined as approximately 2, suggesting the control of the prepared glasses' crystallization via a mechanism that is mono-dimensional in nature [48–50].



**Fig. 4** DSC thermograms for the glass ( $x = 5$ ) at various heating speeds (a) and plot of  $\ln(T_p^2/\beta)$  as a function of inverse temperature for the glass (b)

**Table 4** Crystallization temperature of the glass ( $x = 5 \text{ mol\%}$ ) at different heat crystallization rates

Glass	$\beta$ ( $^{\circ}\text{C}/\text{min}$ )	$T_p$	$\Delta T$	Avrami parameter ( $n$ )
$20\text{Na}_2\text{O}-45\text{Na}_2\text{WO}_4-5\text{TiO}_2-30\text{P}_2\text{O}_5$	5	558	18	2.43
	8	566	20	2.25
	10	570	21	2.17
	12	573	23	2.01

### 4 Conclusion

A number of approaches were employed to facilitate the examination of the prepared glasses.  $\text{TiO}_2$ 's insertion within the glassy framework led to the formation of a P–O–Ti link, the conversion of metaphosphate units to orthophosphate and pyrophosphate units, and an increase in NBOs. The chemical durability suggests that the elaborated glasses are divided into two stages: the first is characterized by a rapid change as a result of the thermodynamic disequilibrium that developed between the solution and the glassy surface. The second is characterized by a slow change as a result of the thermodynamic disequilibrium that developed between the solution (water) and the glassy surface. The saturation of the modifying solution identifies the second. Due to the saturation phenomena, a protective barrier against diffusion is produced on the glassy surface (protective layer). Differential scanning calorimetry was also used to assess crystallization kinetics. The results showed that the crystallization activation energy ( $E_c$ ) was affected by the glassy composition. It was discovered that the glass ( $x = 5 \text{ mol\%}$ ) has an  $E_c$  of  $144.77 \text{ kJ/mol}$  and an Avrami parameter ( $n$ ) of about 2. Based on this, a mono-dimensional periodic landscape may have controlled the crystallization of the glasses. The research on the mechanics of ion transportation into glasses will be the focus of our future work.

## Acknowledgements

M.I. Sayyed and S. Hashim gratefully acknowledge Universiti Teknologi Malaysia for providing Prominent Visiting Researcher Scheme (RJ3000.7113.3F000) initiatives under the Department Deputy of Vice-Chancellor (Research and Innovation).

## Author contributions

All authors contributed to the study conception and design. Material preparation, data collection and analysis were performed by HE, MIS, and LB. The first draft of the manuscript was written by HE and all authors commented on previous versions of the manuscript. All authors read and approved the final manuscript.

## Funding

The authors have not disclosed any funding.

## Data availability

No data were used for the research described in the article.

## Declarations

**Conflict of interest** The authors have no relevant financial or non-financial interests to disclose. The authors have no competing interests to declare that are relevant to the content of this article. All authors certify that they have no affiliations with or involvement in any organization or entity with any financial interest or non-financial interest in the subject matter or materials discussed in this manuscript. The authors have no financial or proprietary interests in any material discussed in this article.

**Research involving human participants and/or animals** This article does not contain any studies involving human participants performed by any of the authors.

## References

1. J.W. Fergus, Ion transport in sodium ion conducting solid electrolytes. *Solid State Ionics* **227**, 102–112 (2012)
2. Y. Wang, S. Song, C. Xu, N. Hu, J. Molenda, L. Lu, Development of solid-state electrolytes for sodium-ion battery—a short review. *Nano Mater. Sci.* **1**(2), 91–100 (2019)
3. Z. Yan, Y. Liang, J. Xiao, W. Lai, W. Wang, Q. Xia et al., A high-kinetics sulfur cathode with a highly efficient mechanism for superior room-temperature Na–S batteries. *Adv. Mater.* **32**(8), 1906700 (2020)
4. H.A. Thabit, N.A. Kabir, N.M. Ahmed, Synthesis and thermoluminescence characteristics and structural and optical studies of ZnO/Ag/ZnO system for dosimetric applications. *J. Lumin.* **236**, 118097 (2021)
5. P.J. Melling, A.R. Allnatt, Modelling of leaching and corrosion of glass. *J. Non-Cryst. Solids* **42**(1–3), 553–559 (1980)
6. E. Fernández, F.J. Gil, M.P. Ginebra, F.C.M. Driessens, J.A. Planell, S.M. Best, Calcium phosphate bone cements for clinical applications. Part I: solution chemistry. *J. Mater. Sci. Mater. Med.* **10**, 169–176 (1999)
7. H. Eboroff-Heidepriem, W. Seeber, D. Ehrt, Dehydration of phosphate glasses. *J. Non-Cryst. Solids* **163**(1), 74–80 (1993)
8. M.R. Reidmeyer, D.E. Day, Phosphorus oxynitride glasses. *J. Non-Cryst. Solids* **181**(3), 201–214 (1995)
9. L. Pascual, A. Durán, Nitridation of glasses in the system R<sub>2</sub>O–MO–P<sub>2</sub>O<sub>5</sub>. *Mater. Res. Bull.* **31**(1), 77–95 (1996)
10. A. Le Sauze, R. Marchand, Chemically durable nitrated phosphate glasses resulting from nitrogen/oxygen substitution within PO<sub>4</sub> tetrahedra. *J. Non-Cryst. Solids* **263**, 285–292 (2000)
11. H.A. Abo-Mosallam, Influences of SrO on the structure, thermo-physical and chemical properties of zinc iron borophosphate glasses as host matrices for radioactive waste. *J. Non-Cryst. Solids* **571**, 121084 (2021)
12. S.V. Pershina, B.D. Antonov, I.I. Leonidov, Effect of MoO<sub>3</sub> on structural, thermal and transport properties of lithium phosphate glasses. *J. Non-Cryst. Solids* **569**, 120944 (2021)
13. A. Ibrahim, M.S. Sadeq, Influence of cobalt oxide on the structure, optical transitions and ligand field parameters of lithium phosphate glasses. *Ceram. Int.* **47**(20), 28536–28542 (2021)
14. H. Es-Soufi, L. Bih, Effect of TiO<sub>2</sub> on the chemical durability and optical properties of Mo-based phosphate glasses. *J. Non-Cryst. Solids* **558**, 120655 (2021)
15. H.A. Thabit, N.A. Kabir, N.M. Ahmed, Synthesis & thermoluminescence characteristics & structural and optical studies of ZnO/Ag/ZnO system for dosimetric applications. *J. Lumin.* **236**, 118097 (2021)

16. H. Segawa, N. Akagi, T. Yano, S. Shibata, Properties and structures of  $\text{TiO}_2\text{-ZnO-P}_2\text{O}_5$  glasses. *J. Ceram. Soc. Jpn.* **118**(1376), 278–282 (2010)
17. H. Es-soufi, L. Ouachou, M.I. Sayyed, S. Hashim, H. Bih, L. Bih, Synthesis and investigation of the physical, structural, and radiation shielding properties of the titano-bismuth phosphate glasses. *J. Mater. Sci. Mater. Electron.* **34**(12), 1040 (2023)
18. I. Mimouni, A. Bouziani, Y. Naciri, M. Boujnah, M.A. El Belghiti, M. El Azzouzi, Effect of heat treatment on the photocatalytic activity of  $\alpha\text{-Fe}_2\text{O}_3$  nanoparticles: towards diclofenac elimination. *Environ. Sci. Pollut. Res.* **29**, 7984–7996 (2021)
19. D.S. Brauer, Bioactive glasses—structure and properties. *Angew. Chem. Int. Ed.* **54**(14), 4160–4181 (2015)
20. A. Kiani, N.J. Lakhkar, V. Salih, M.E. Smith, J.V. Hanna, R.J. Newport et al., Titanium-containing bioactive phosphate glasses. *Philos. Trans. R. Soc. A Math. Phys. Eng. Sci.* **370**(1963), 1352–1375 (2012)
21. E.A. Abou Neel, W. Chrzanowski, J.C. Knowles, Effect of increasing titanium dioxide content on bulk and surface properties of phosphate-based glasses. *Acta Biomater.* **4**(3), 523–534 (2008)
22. T. Kasuga, Y. Abe, Calcium phosphate invert glasses with soda and titania. *J. Non-Cryst. Solids* **243**(1), 70–74 (1999)
23. M. Kaur, A. Singh, V. Thakur, L. Singh, Effect of  $\text{TiO}_2$  substitution on optical and structural aspects of phosphate glasses. *J. Mol. Struct.* **1089**, 95–101 (2015)
24. M. Ataalla, A.S. Afify, M. Hassan, M. Abdallah, M. Milanova, H.Y. Aboul-Enein, A. Mohamed, Tungsten-based glasses for photochromic, electrochromic, gas sensors, and related applications: a review. *J. Non-Cryst. Solids* **491**, 43–54 (2018)
25. H. Es-Soufi, L. Bih, A.R. Lima, A. El Bouari, B. Manoun, S. Hussain, Investigation DSC and XRD on the crystallization kinetics in the phosphate  $\text{Li}_2\text{O-Li}_2\text{WO}_4\text{-TiO}_2\text{-P}_2\text{O}_5$  glassy ionic system. *J. Mater. Sci. Mater. Electron.* (2021). <https://doi.org/10.21203/rs.3.rs-190511/v1>
26. M. Nalin, G. Poirier, S.J.L. Ribeiro, Y. Messaddeq, L. Cesca, Glasses in the  $\text{SbPO}_4\text{-WO}_3$  system. *J. Non-Cryst. Solids* **353**(16–17), 1592–1597 (2007)
27. D. Boudlich, L. Bih, M.E.H. Archidi, M. Haddad, A. Yacoubi, A. Nadiri, B. Elouadi, Infrared, Raman, and electron spin resonance studies of vitreous alkaline tungsten phosphates and related glasses. *J. Am. Ceram. Soc.* **85**(3), 623–630 (2002)
28. K.C. Sekhar, A. Hameed, N. Narsimlu, J.S. Alzahrani, M.A. Alothman, I.O. Olarinoye et al., Synthesis, optical, structural, and radiation transmission properties of  $\text{PbO/Bi}_2\text{O}_3/\text{B}_2\text{O}_3/\text{Fe}_2\text{O}_3$  glasses: an experimental and in silico study. *Opt. Mater.* **117**, 111173 (2021)
29. H. Es-soufi, L. Bih, Synthesis, characterization, and optical properties of titano-molybdenum phosphate glasses. *J. Electron. Mater.* **51**(5), 2528–2544 (2022)
30. A. Rezikyan, G.G. Moore, Fluctuation electron microscopy study of crystal nucleation in  $\text{TiO}_2\text{-SiO}_2$  glass with heat treatment. *J. Phys. Condens. Matter* **32**(48), 485402 (2020)
31. H.A. Thabit, A.K. Ismail, M.I. Sayyed, H. Es-soufi, Preparation, characterization, and mechanical-optical properties of telluro-borate glasses containing tungsten. *Ceram. Int.* (2023). <https://doi.org/10.1016/j.ceramint.2023.05.185>
32. R. Pagoti, S. Panda, V. Patchpureddy, R.K. Padhi, B. Subramanian, H. Jena, B.S. Panigrahi, Structural and spectroscopic investigations of neodymium-doped strontium borophosphate glass. *Luminescence* **36**(7), 1706–1715 (2021)
33. M. Nagarjuna, T. Satyanarayana, Y. Gandhi, N. Veeraiiah, Influence of  $\text{Ag}_2\text{O}$  on some physical properties of  $\text{LiF-TiO}_2\text{-P}_2\text{O}_5$  glass system. *J. Alloys Compd.* **479**(1–2), 549–556 (2009)
34. R.K. Brow, D.R. Tallant, S.T. Myers, C.C. Phifer, The short-range structure of zinc polyphosphate glass. *J. Non-Cryst. Solids* **191**(1–2), 45–55 (1995)
35. Z. Černošek, M. Chládková, J. Holubová, The influence of  $\text{TiO}_2$  on the structure and properties of sodium-zinc phosphate glasses. *J. Non-Cryst. Solids* **531**, 119866 (2020)
36. F. Delahaye-Carrière, Doctoral dissertation Compiègne (1997)
37. L. Ma, R.K. Brow, M.E. Schlesinger, Dissolution behavior of  $\text{Na}_2\text{O-FeO-Fe}_2\text{O}_3\text{-P}_2\text{O}_5$  glasses. *J. Non-Cryst. Solids* **463**, 90–101 (2017)
38. M.N. Rahaman, *Ceramic Processing and Sintering*, 2nd edn. (Marcel Dekker, New York, 2003)
39. Y. Gu, W. Xiao, L. Lu, W. Huang, M.N. Rahaman, D. Wang, Kinetics and mechanisms of converting bioactive borate glasses to hydroxyapatite in aqueous phosphate solution. *J. Mater. Sci.* **46**, 47–54 (2011)
40. H. Es-soufi, H. Bih, M. Azrou, B. Manoun, P. Lazor, Structure and some physical properties of the sodium ion conducting glasses inside the  $\text{Na}_2\text{O-Na}_2\text{WO}_4\text{-TiO}_2\text{-P}_2\text{O}_5$  system. *J. Appl. Surf. Interfaces* (2018). <https://doi.org/10.48442/IMIST.PRSM/jasi-v4i1-3.11273>
41. R.N. Oosterbeek, K.I. Margaritis, X.C. Zhang, S.M. Best, R.E. Cameron, Non-linear dissolution mechanisms of sodium calcium phosphate glasses as a function of pH in various aqueous media. *J. Eur. Ceram. Soc.* **41**(1), 901–911 (2021)
42. C. Solenn, thèse de doctorat Université Rennes 1 (2016)
43. N. Mascaraque, A. Durán, F. Muñoz, Effect of fluorine and nitrogen on the chemical durability of lithium phosphate glasses. *J. Non-Cryst. Solids* **417**, 60–65 (2015)

44. H.E. Kissinger, Differential thermal analysis. *J. Res. Natl. Bur. Stand.* **57**(4), 217 (1956)
45. J.A. Augis, J.E. Bennett, Calculation of the Avrami parameters for heterogeneous solid state reactions using a modification of the Kissinger method. *J. Therm. Anal.* **13**, 283–292 (1978)
46. D.R. Lide (ed.), *CRC Handbook of Chemistry and Physics* (CRC Press, Boca Raton, 2001)
47. M. Avrami, Kinetics of phase change 1. *J. Chem. Phys.* **7**, 1103 (1939)
48. M. Avrami, *J. Chem. Phys.* **8**, 212 (1940)
49. M. Avrami, *J. Chem. Phys.* **9**, 177 (1941)
50. N. Elkhoshkhany, E. Syala, Kinetic characterization of  $\text{TeO}_2$ – $\text{Bi}_2\text{O}_3$ – $\text{V}_2\text{O}_5$ – $\text{Na}_2\text{O}$ – $\text{TiO}_2$  glass system. *Ceram. Int.* **43**(8), 6156–6162 (2017)

**Publisher's Note** Springer Nature remains neutral with regard to jurisdictional claims in published maps and institutional affiliations.

Springer Nature or its licensor (e.g. a society or other partner) holds exclusive rights to this article under a publishing agreement with the author(s) or other rightsholder(s); author self-archiving of the accepted manuscript version of this article is solely governed by the terms of such publishing agreement and applicable law.